12-10-2013

Evolution of the superconductivity dome in the two-dimensional Hubbard model

K. S. Chen
Louisiana State University

Z. Y. Meng
Louisiana State University

S. X. Yang
Louisiana State University

T. Pruschke
Georg-August-Universität Göttingen

J. Moreno
Louisiana State University

See next page for additional authors

Recommended Citation

Chen, K., Meng, Z., Yang, S., Pruschke, T., Moreno, J., & Jarrell, M. (2013). Evolution of the superconductivity dome in the two-dimensional Hubbard model. *Physical Review B - Condensed Matter and Materials Physics, 88* (24) https://doi.org/10.1103/PhysRevB.88.245110

Evolution of the Superconductivity Dome in the two dimensional Hubbard Model

K.-S. Chen,[1,*] Z. Y. Meng,[1,2,†] S.-X. Yang,[1,2] T. Pruschke,[3] J. Moreno,[1,2] and M. Jarrell[1,2]

[1] *Department of Physics and Astronomy, Louisiana State University, Baton Rouge, LA 70803, USA*
[2] *Center for Computation and Technology, Louisiana State University, Baton Rouge, LA 70808, USA*
[3] *Department of Physics, University of Göttingen, D-37077 Göttingen, Germany*

(Dated: September 17, 2018)

In a recent publication [Chen *et al.*, Phys. Rev. B **86**, 165136 (2012)], we identified a line of Lifshitz transition points separating the Fermi liquid and pseudogap regions in the hole-doped two dimensional Hubbard model. Here we extend the study to further determine the superconducting transition temperature in the phase diagram. By means of large-scale dynamical cluster quantum Monte Carlo simulations, we are able to identify the evolution of the d-wave superconducting dome in the hole-dope side of the phase diagram, with next-nearest-neighbor hopping (t'), chemical potential and temperature as control parameters. To obtain the superconducting transition temperature T_c, we employ two-particle measurements of the pairing susceptibilities. As t' goes from positive to negative values, we find the d-wave projected irreducible pairing vertex function is enhanced, and the curvature of its doping dependence changes from convex to concave, which fixes the position of the maximum superconducting temperature at the same filling ($n \approx 0.85$) and constraints the dome from precisely following the Lifshitz line. We furthermore decompose the irreducible vertex function into fully irreducible, charge and spin components via the parquet equations, and consistently find that the spin component dominates the pairing vertex function in the doping range where the dome is located. Our investigations deepen the understanding of the phase diagram of the two dimensional Hubbard model, and more importantly pose new questions to the field. For example, we found as t' goes from positive to negative values, the curvature of the pairing strength as a function of doping changes from convex to concave, and the nature of the dominant fluctuations changes from charge degree of freedom to spin degree of freedom. The study of these issues will lead to further understanding of the phase diagram of the two dimensional Hubbard model and also the physics of the hole-doped cuprate high temperature superconductors.

PACS numbers: 74.40.Kb, 71.10.Fd, 74.72.-h, 71.10.Hf

I. INTRODUCTION

The phase diagram of the hole-doped two-dimensional Hubbard model in the strongly correlated regime contains many interesting features resembling those observed in the high-Tc cuprate superconductors[1,2]. At a qualitative level, it is accepted that the generic ingredients of the cuprate physics are captured by the one band Hubbard model on the square lattice[3,4]. For example, the Fermi surface reconstruction is observed in the study of the Hubbard model on the square lattice as the doping concentration is varied[5,6]. Starting from the overdoped Fermi liquid, with an electron-like Fermi surface, quadratic resistivity in temperature and well-defined quasiparticles, the system exhibits around optimal doping for the temperature regime studied a vanishing quasiparticle weight on the Fermi surface and a linear resistivity, reminiscent of a marginal Fermi liquid[7,8]. At smaller doping concentrations, the system enters a pseudogap region where the density of states is further suppressed close to the Fermi level, and the topology of the Fermi surface changes to hole-like. Eventually at half-filling, a Mott gap opens and antiferromagnetic order sets in.

Among the many interesting questions concerning the phase diagram of the hole-doped Hubbard model on a square lattice, the presence of the d-wave superconducting dome, as observed in the cuprate superconductors, is the central one. It is commonly accepted that the physics of cuprates is due to moderate to strong electronic correlations. Therefore, any study of low-temperature properties faces the difficulty that one cannot employ conventional perturbative methods to obtain reliable information. In this paper, we address the existence of a d-wave superconductivity dome in the Hubbard model directly using large-scale dynamical cluster quantum Monte Carlo simulations[9–12]. Based on the understanding obtained in this and previous numerical works [5,6,13–25], we furthermore map the evolution of the d-wave superconductivity dome in the parameter space of the phase diagram.

In order to put this work into the proper perspective, it is worthwhile to recapitulate our knowledge about the phase diagram of the two-dimensional Hubbard model. Using large-scale dynamical cluster quantum Monte Carlo simulations, the phase diagram of the two-dimensional Hubbard model near quantum critical filling (optimal filling or doping) was mapped out in a series of numerical works [5,6,13–15,17,21,22]. The control parameters are the next-nearest-neighbor hopping (t'/t), chemical potential (or doping concentration) and temperature. At positive t', there is a first-order phase separation transition occurring at finite temperature. The two phases being separated are an incompressible Mott liquid and a compressible Mott gas; these two phases are adiabatically connected to the pseudogap and the Fermi liquid states at $t' = 0$. The first order line of coexis-

tence terminates at a second order point where the charge susceptibility diverges[13,15,17,22]. As $t' \to 0$, this critical point extrapolates continuously to zero temperature and thus becomes the quantum critical point (QCP) underneath the superconducting dome[21]. Above the QCP, a V-shaped quantum critical region separates the pseudogap and the Fermi liquid phases [5,14].

When the next-nearest-neighbor hopping becomes negative, $t' < 0$, which is relevant for the hole-doped cuprates, the physics becomes more interesting[5,6]. We find at $t'/t \leq 0$, as the doping concentration varies from the overdoped to the underdoped regime, the Fermi surface changes its topology from electron-like with complete Fermi surface to hole-like with a pseudogap in the anti-nodal direction. Such a topological transition in the Fermi surface is a Lifshitz transition[6,26–29]. It is furthermore concomitant with a van Hove singularity in the density of states crossing the Fermi level at a doping which occurs very close to (if not at) the quantum critical point. Interestingly, we find the quantum critical phenomena prevail along the line of Lifshitz transition for negative t'. The temperature dependence of the correlation effects close to the van Hove singularities, and its influence on quantities like the quasiparticle fraction and the pairing polarization are very different from those found in the traditional van Hove scenarios[30,31].

A schematic phase diagram based on these studies is provided in Fig. 8 of Ref. 6. However, the position of the superconducting dome and its evolution in the negative t' side of the phase diagram have not been addressed. From our previous work[6,21] we understand that the formation of the d-wave superconducting dome is due to two competing factors: the effective pairing strength V_d and the d-wave pairing bubble χ_d^0. When $t' = 0$, V_d decreases monotonically as a function of doping while the χ_d^0 shows algebraic divergence ($\frac{1}{\sqrt{T}}$) near the quantumcritical doping (Lifshitz doping) and a much slower dependence in the pseudogap and Fermi liquid regions. The combined effect of the monotonic decay of V_d and the algebraic divergence of χ_d^0 results in the maximum of the dome occurring near the critical doping.

In this paper we extend the study of the d-wave pairing and the superconducting dome to the negative t' side of the phase diagram. To this end, we include extensive two-particle measurements into the dynamical cluster quantum Monte Carlo simulations. This allows to measure the d-wave pairing susceptibility directly, and obtains the superconducting transition temperature T_c from its divergence. We find that the superconducting dome is located around the quantum critical doping, and furthermore follows its evolution into negative t' values. The evolution of the dome is subtle, in the sense that its peak stays close to the same filling ($n \approx 0.85$), whereas the whole dome moves outside towards higher doping, following the direction of the Lifshitz line. The d-wave projected irreducible pairing vertex function (the effective pairing strength V_d) is enhanced as t' changes from positive to negative values, in the under- and optimal-doped regions. The doping dependence of the effective pairing strength, changes its curvature from convex to concave as t' goes to negative values, which fixes the position of the maximum superconducting temperature (the peak of the dome) at the same filling ($n \approx 0.85$) and constraints the dome from precisely following the Lifshitz line. Therefore, the asymmetry of the superconducting dome becomes more pronounced when t' goes to negative values due to the non-trivial doping dependence of V_d. The vertex decomposition via parquet equations furthermore reveals that in the negative t' side of the phase diagram, the effective pairing strength is dominated by magnetic fluctuations associated with the antiferromagnetic order at momentum transfer $\mathbf{Q} = (\pi, \pi)$.

The paper is organized as follows. Section II outlines the model and the methods used in this study: the dynamical cluster approximation (DCA) with weak-coupling continuous-time quantum Monte Carlo (CTQMC) as its cluster solver. We explain in detail how the two-particle vertex function and its decomposition has been included into our DCA/CTQMC simulations. Section III and IV contain our numerical results and discussion, beginning with d-wave pairing susceptibility and the evolution of the superconducting dome as a function of t'/t, and followed by a detailed account of the irreducible pairing vertex function and its decomposition via parquet equations. We then provide results on the cluster spin susceptibility at a fixed filling and various t'/t. We use a schematic quantum critical phase diagram of the model to summarize our results. We end with conclusions and an overview of open questions in Section V.

II. FORMALISM

The model we study in this paper is the Hubbard model on a square lattice

$$H = \sum_{\mathbf{k}\sigma} \left(\epsilon_{\mathbf{k}}^0 - \mu\right) c_{\mathbf{k}\sigma}^\dagger c_{\mathbf{k}\sigma} + U \sum_i n_{i\uparrow} n_{i\downarrow}, \qquad (1)$$

where $c_{\mathbf{k}\sigma}^\dagger (c_{\mathbf{k}\sigma})$ is the creation (annihilation) operator for electrons with wavevector $\mathbf{k}$ and spin σ, μ is the chemical potential, $n_{i\sigma} = c_{i\sigma}^\dagger c_{i\sigma}$ is the number operator, U is the on-site Coulomb repulsion, and the bare dispersion is given by

$$\epsilon_{\mathbf{k}}^0 = -2t\left(\cos k_x + \cos k_y\right) - 4t' \cos k_x \cos k_y, \qquad (2)$$

with t and t' being the hopping amplitudes between nearest and next-nearest-neighbor sites respectively.

We use the DCA[9,10] with interaction-expansion CTQMC[32] as a cluster solver. The DCA is a mean-field theory on clusters that maps the lattice of the original system onto a periodic cluster of size $N_c = L_c^D$ (D is the dimensionality) embedded in a self-consistently determined host. The spatial short-ranged correlations (up

to L_c) are treated explicitly while the long-ranged correlations are taken into account in a mean-field approximation. In this paper we study cluster sizes of $N_c = 12$ and 16, and compared results with other cluster sizes in previous studies[5,6,14,15,17,21,22,33]. The energy unit is $4t = 1$, and the interaction strength is set as $U = 6t$. The interaction-expansion CTQMC solver treats the temporal correlations, especially important for quantum criticality, for all cluster sizes. In our simulation, we can achieve temperatures as low as $T = 0.04t$ ($\beta t = 22.5$) before a serious minus-sign problem renders the data untrustable.

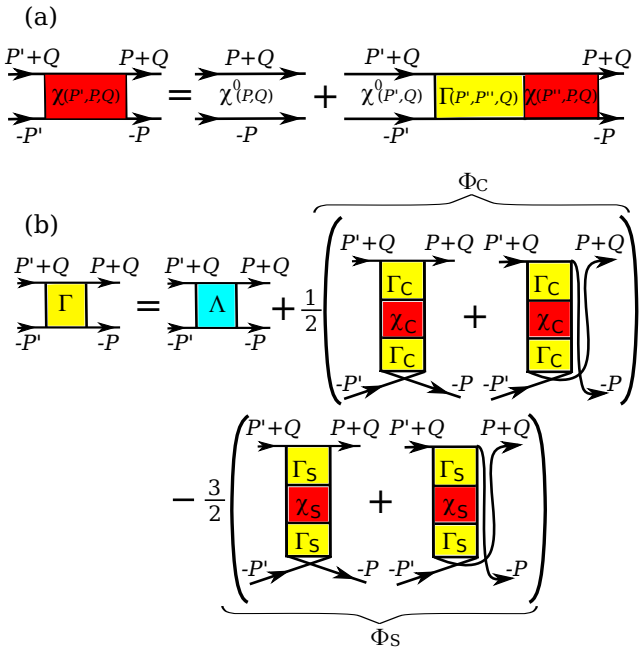

FIG. 1. (color online) (a) Bethe Salpeter equation for the particle-particle pairing channel. $\chi(P, P', Q)$ is the two particle Green function and $\Gamma(P', P", Q)$ is the irreducible vertex function, both are defined on the DCA/CTQMC cluster. $\chi^0(P, Q)$ is the bare bubble coarse-grained from lattice to cluster. (b) Decomposition of the irreducible particle-particle vertex Γ into a fully irreducible vertex Λ and cross channel contributions from charge Φ_C and spin Φ_S components. Both Φ_C and Φ_S come from the particle-hole channel with $\chi_{S/C}$ and $\Gamma_{C/S}$ as the corresponding two-particle Green functions and irreducible vertex functions extracted from their own Bethe Salpeter equations, similarly as that in (a).

The self-consistent loop of the DCA is built at the single-particle level, hence we can obtain the lattice Green function $G(\mathbf{k}, i\omega_n)$ and self-energy $\Sigma(\mathbf{k}, i\omega_n)$, and perform their analytical continuation using the Maximum Entropy Method (MEM)[5,6,34,35] to obtain the real-frequency single-particle quantities such as $G(\mathbf{k}, \omega)$, $\Sigma(\mathbf{k}, \omega)$, local density of states $N(\omega)$ and spectral function $A(\mathbf{k}, \omega)$. However, to obtain various susceptibilities and vertex functions, we need to go to the two-particle level in our DCA/CTQMC simulations. To this end, we measure the two-particle Green function, $\chi(P, P', Q)$, where the four-momentum notation $P \equiv (\mathbf{K}, i\omega_n)$ and $Q \equiv (\mathbf{Q}, i\nu_m)$ are introduced, with $\mathbf{K}$, $\mathbf{Q}$ are momentum points on the cluster, and $\omega_n = (2n + 1)\pi T$ and $\nu_m = 2m\pi T$ are fermionic and bosonic Matsubara frequencies, respectively. From the two-particle Green function, we extract the irreducible vertex function, $\Gamma(P, P', Q)$, via the Bethe-Salpeter equation. Fig. 1 (a) demonstrates an example of the Bethe-Salpeter equation in the particle-particle pairing channel. The bare bubble $\chi^0(P, Q) = G(-P)G(P + Q)$ entering the Bethe-Salpeter equation is obtained from the fully dressed single-particle Green function, coarse-grained from lattice to cluster. Once we have the irreducible vertex, Γ, the lattice susceptibility can be calculated from $\chi(T) = \dfrac{\chi^0}{1 - \Gamma\chi^0}$, where the summation is over all the frequency and momentum indices. Since the square lattice Hubbard model exhibits d-wave superconductivity, the lattice d-wave susceptibility, $\chi_d(T)$, is obtained by projecting the pairing susceptibility with the d-wave form factor $g_d(\mathbf{k}) = \cos(k_x) - \cos(k_y)$ via $\chi_d(T) = \sum_{\mathbf{k},\mathbf{k}'} g_d(\mathbf{k})\chi_{\mathbf{k},\mathbf{k}'}(T)g_d(\mathbf{k}')/\sum_{\mathbf{k}} g_d^2(\mathbf{k})$. The superconducting transition temperature can be determined by extrapolating $1/\chi_d(T)$ to zero.

To further explore the pairing mechanism, we decompose the irreducible pairing vertex Γ, by means of the parquet equation[21,33,36–38], into three independent contributions, $\Gamma = \Lambda + \Phi_C + \Phi_S$, as shown in Fig. 1 (b). These three contributions are the fully irreducible vertex Λ, the charge ($S = 0$) component Φ_C, and the spin ($S = 1$) component Φ_S. We further project both sides of the equation with the d-wave form factor. For example, the effective d-wave pairing strength, is given by $V_d = \sum_{\mathbf{k},\mathbf{k}'} g_d(\mathbf{k})\Gamma_{\mathbf{k},\mathbf{k}'}g_d(\mathbf{k}')/\sum_{\mathbf{k}} g_d^2(\mathbf{k})$. Such vertex decomposition approach tells which component contributes most to the irreducible pairing vertex. One important point to note is that as we have controlled information about the two particle vertex function in momentum and frequency, we do not need to assume any kind of pairing mechanism a priori, but can numerically identify the channel which is dominant in the pairing interaction. This is a qualitative improvement over typical effective weak-coupling approaches where one channel (usually spin) is always assumed to dominate. As it will become clear later, we have obtained convincing numerical evidence that, at $t'/t \leq 0$, the spin component Φ_S not only dominates Γ but also has the maximum value with the momentum transfer $\mathbf{Q} = (\pi, \pi)$, revealing that the superconducting pairing strength is mainly due to the antiferromagnetic fluctuations.

III. RESULTS

The left panel of Fig. 2 displays the d-wave pairing susceptibility for $t'/t = -0.1$ and doping concentration varying from half-filling to overdoped. Also, results for $t' = 0$ at $n = 0.85$ are shown. At or close to half-filling, $n = 1.0$, 0.95, where the system is inside the insulating

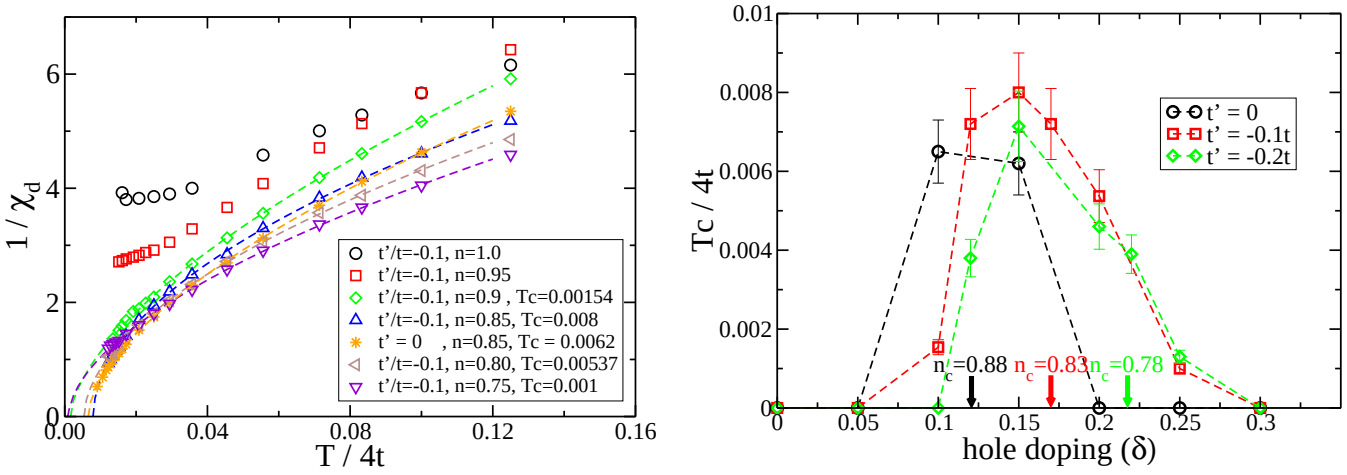

FIG. 2. (color online) Left panel: d-wave pairing susceptibility at $t'/t = -0.1$ and various doping concentrations (also one data set for $t' = 0$ at $n = 0.85$). The extrapolated transition temperature T_c follows a dome shape curve between the fillings of $n = 0.9$ (doping $\delta = 0.1$) and $n = 0.75$ (doping $\delta = 0.25$), with its peak locates close to filling $n = 0.85$. Right panel: Extrapolated d-wave superconducting transition temperature T_c for $t'/t = 0$, -0.1 and -0.2. The bold arrows indicate the corresponding quantum critical filling (n_c) along the Lifshitz line, determined in our previous work[6]. The error bars of T_c are obtained from the extrapolation of the T_c for independent DCA/CTQMC simulations. The dome shifts towards higher doping as t'/t becomes negative, but the peak of the dome is always located close to $\delta = 0.15$. Results are obtained from $N_c = 12$ and 16 DCA/CTQMC simulations.

or the pseudogap regions, the pairing susceptibility does not diverge at low temperatures. By increasing the doping beyond $n = 0.9$ the pairing susceptibility becomes diverging at a finite T_c. The value of T_c grows as the doping level changes from underdoped toward optimal doping at filling $n = 0.85$. For higher doping, T_c decreases and the d-wave superconducting dome eventually takes shape. Interestingly, above the optimal doping, we have observed marginal Fermi liquid behavior with self-energy linear on frequency and resistivity linear on temperature[5,6,15].

The right panel of Fig. 2 shows the extrapolated T_c as function of doping for $t'/t = 0$, -0.1 and -0.2. Two interesting observations can be made. First, as t'/t becomes negative, the d-wave superconducting transition temperature increases, while the highest T_c occurs around $n = 0.85$. For more negative values of t'/t, e.g., -0.3, -0.4, T_c decreases. Therefore, the superconducting dome evolves into a mountain-type volume in the δ vs t'/t phase diagram. Second, we find that as t'/t becomes more negative, the superconducting dome moves slightly towards higher doping. At first glance, this behavior seems to resemble the one of the Lifshitz line identified in Ref. 6. The Lifshitz line traces those values of doping and t'/t where the interaction-induced van Hove singularity crosses the Fermi level. Note we have pointed out the correspond quantum critical Lifshitz fillings, n_c, for $t'/t = 0$, -0.1 and -0.2 by bold arrows in the right panel of Fig. 2. Naively, one would expect the Lifshitz filling to be associated with the maximum pairing interaction and transition temperature. However, inspecting

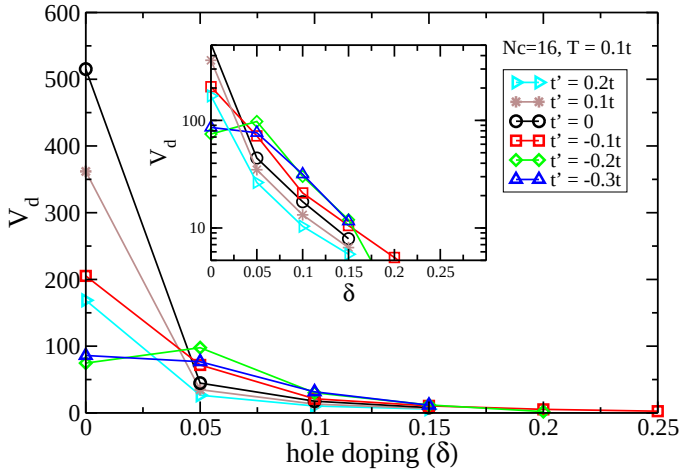

FIG. 3. (color online) Evolution of the d-wave projected irreducible vertex function, V_d, as a function of hole-doping for various t'/t. At half-filling, V_d is strongest at $t' = 0$ and decays for both positive and negative t'. In the underdoped region (doping $\delta = 0.05$, 0.1 and 0.15), V_d is an increasing function as t' varies from positive to negative. The inset presents the same data in a semi-log plot and the enhancement of V_d from $t' > 0$ to $t' < 0$ can be clearly seen. Also note that the curvature of the doping dependence of V_d changes from convex to concave when t' becomes negative.

the behavior more quantitatively, the maximum of the dome actually stay close to n=0.85 and does not fully follow the Lifshitz line. We thus have to conclude that

the interaction-induced van Hove singularity alone does not determine the superconducting transition, at least not the position of the highest transition temperature.

To understand this behavior, we explore the projected irreducible d-wave pairing vertex, V_d, as function of doping for various t'/t using a $N_c = 16$ site cluster and temperature $T = 0.1t$ (Figure 3). Since V_d is the effective pairing strength, the BCS condition $V_d\chi_d^0 = 1$ is roughly equivalent to the divergence of the d-wave pairing susceptibility[21,39]. In our previous work[6,21], we found that at $t' = 0$ V_d decays monotonically as a function of doping, forming a convex function. χ_d^0 has an algebraic temperature dependence at the quantum critical filling and is much less sensitive to temperature at other fillings. The combined doping dependence of V_d and χ_d^0 gives rise to the superconducting dome at $t' = 0$ with its peak located close to the quantum critical filling. Here, as shown in Fig. 3, we find that V_d develops a more complicated doping dependence for different values of t'. In general, it is largest at half-filling and decays to smaller values at larger doping. However, V_d displays non-trivial features in the underdoped and optimally doped regions. The inset to Fig. 3, where the data are presented in semi-log fashion, shows that for doping $\delta = 0.05$, 0.1, and 0.15 the value of V_d systematically increases when t'/t goes from positive to negative values. In particular, at $\delta = 0.05$ and $t'/t = -0.2$, the value of V_d is larger than that at half filling. The curvature of the doping dependence of the effective pairing strength, $V_d(\delta)$, changes from a convex function for $t' \geq -0.1$ to a concave one for $t' < -0.1$. However, the enhancement of V_d stops beyond $t' = -0.3t$, and V_d starts to strongly decrease also as a function of t'/t.

Putting all these observations together, it is evident that V_d develops a non-trivial landscape as function of δ and t'/t. At half-filling, V_d is largest for $t' = 0$, and decays as $|t'/t|$ increases. This behavior is easily understood as t' introduces frustration into the system and suppresses the tendency towards antiferromagnetic order. This symmetry is destroyed for finite doping. In the underdoped and optimally doped region, V_d is enhanced as t'/t goes from positive to negative values, and finally decays once t'/t becomes very negative. Furthermore, the doping dependence of V_d, changes from a convex to a concave function for negative t'/t. We think the concave curvature of V_d at negative t' is responsible for the fixed position of the peak in the superconducting dome at different t'. In addition, the faster decay of V_d with doping at negative t', due to its concave nature, actually constraints the dome to be further pushed to higher doping, even though the Lifshitz line moves towards higher doping at negative t'. The different behaviors of V_d for positive and negative t' reflects the previous observation that in lieu of superconductivity the states in those two regions are fundamentally different. For example for n=0.85, the system is a Fermi liquid state for $t' > 0$, while it resides in the pseudogap phase for $t' < 0$[6].

To furthermore explore the pairing mechanism, we performed a decomposition of the irreducible pairing vertex Γ via the parquet equations[33,37,38] as described in section II. The results are shown in Fig. 4. The left panel is the vertex decomposition for filling $n = 0.9$ and $t'/t = -0.1$, 0 and 0.1. The behavior of Γ is consistent with the one of V_d from Fig. 3. For a fixed temperature, Γ increases as t'/t changes from 0.1 to -0.1, and the increase becomes enhanced at lower temperatures. The dominant contribution to Γ for $t'/t = -0.1$, 0 and 0.1 comes from the $S = 1$ magnetic component Φ_S. The same observations hold for the right panel of Fig. 4, which corresponds to a filling $n = 0.85$. In fact, we also find from the vertex decomposition that the momentum dependence of Φ_S is peaked at the momentum transfer $\mathbf{Q} = (\pi, \pi)$, associated with the antiferromagnetic fluctuations of the square lattice[33].

To clearly demonstrate the difference in the antiferromagnetic fluctuations at $t' > 0$ and $t' < 0$, we measure the cluster spin susceptibility $\chi_S(\mathbf{Q}, T)$ for $N_c = 16$, filling $n = 0.85$ (doping $\delta = 0.15$), and temperature $T = 0.1t$, and we interpolate $\chi_S(\mathbf{Q}, T)$ throughout the entire Brillouin Zone (BZ). The results are shown in Fig. 5. As one can see, $\chi_S(\mathbf{Q} = (\pi, \pi))$ becomes stronger as t'/t goes from positive (0.2) to negative (-0.3) values, i.e. the antiferromagnetic fluctuations are indeed stronger for the negative t' side. Together with the findings for the pairing strength V_d and the decomposition of the irreducible pairing vertex Γ into its different components, the behavior of the spin susceptibility makes the picture clearer. As mentioned previously, the system is a conventional Fermi liquid for $t' > 0$, but in the pseudogap phase for $t' < 0$. Obviously, the different physical properties are intimately connected with the spin fluctuations, as Fig. 5 shows. From Fig. 4 of our previous publication[6], we learned that the Fermi surface for $n = 0.85$ is electron-like at $t' > 0$ and hole-like at $t' < 0$. The electron-like Fermi surface does not occupy the regions in the BZ close to $(\pi, 0)$ and $(0, \pi)$, hence the system cannot respond to the antiferromagnetic fluctuations; however, for the hole-like Fermi surface, regions close to $(\pi, 0)$ and $(0, \pi)$ are occupied, and the electrons there can couple to the antiferromagnetic fluctuation efficiently. From the vertex decomposition in Fig. 4 we also know that the antiferromagnetic fluctuations are strongest at the momentum transfer connecting $(\pi, 0)$ and $(0, \pi)$. Hence, for $t' > 0$ the system at optimal filling $n = 0.85$ is a stable Fermi liquid, whereas for $t' < 0$ it is already inside the pseudogap region with electrons at the antinodal $(\pi, 0)$ to $(0, \pi)$ momenta coupled strongly by antiferromagnetic fluctuations.

Previous studies[40] have suggested that for strongly negative t' (> -0.5) and close the so-called van-Hove filling, a ferromagnetic phase with a tendency towards p-wave superconductivity might appear. It surely is interesting to investigate whether this weak coupling prediction for large negative values of t' is still valid in the strongly correlated system we study here.

To further probe our model we calculate the bulk spin

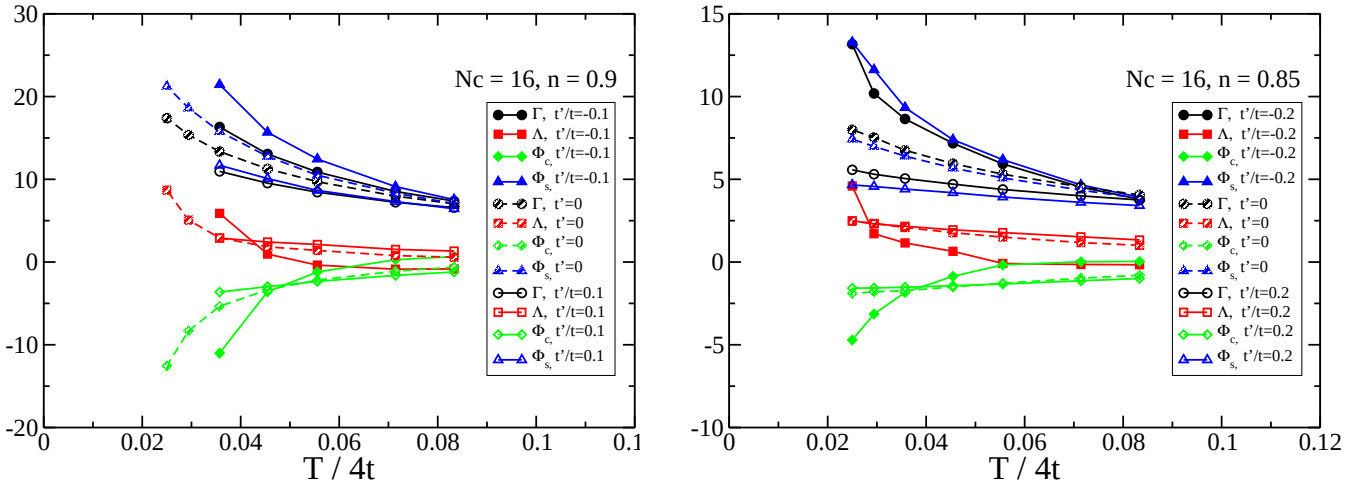

FIG. 4. (color online) Decomposition of the irreducible pairing vertex Γ into fully irreducible Λ, charge Φ_C and spin Φ_S contributions. (Left panel) Decomposition for filling $n = 0.9$ (doping $\delta = 0.1$) at $t'/t = -0.1, 0$ and 0.1. (Right panel) Decomposition for filling $n = 0.85$ (doping $\delta = 0.15$) at various $t'/t = -0.2, 0$ and 0.2. In both cases, the $S = 1$ magnetic components Φ_S are the dominant contribution to the irreducible pairing vertex.

and charge susceptibilities. Fig. 6 (a), (b) and (c) show the bulk spin susceptibility, $\chi_S(\mathbf{Q} = 0, T)$, at different $t'/t = 0$, -0.1 and -0.2 and fillings $n = 0.95, 0.90, 0.85$ and the corresponding quantum critical Lifshitz filling at that value of t'/t, $n_c(t'/t)$. Panels (d), (e), and (f) display $\chi_S(\mathbf{Q} = 0, T)$ for the same values of t'/t and filling. The maximum of the bulk spin susceptibility is used to determine the pseudogap temperature T^*[14,23,41]. One can see in all the three cases, T^* is highest close to half-filling ($n = 0.95$), and gradually reduces as the doping increases. The lines with star symbols correspond to the Lifshitz filling[6], $n_c(t'/t)$, at which the Fermi surface changes its topology from electron-like to hole-like. As we have pointed out previously[6], the slope of T^* as a function of doping δ becomes less steep as t' goes to negative values, which means that the quantum critical region in the phase diagram becomes wider on the negative t' side; it is also interesting that for negative t', $\chi_S(\mathbf{Q} = 0, T)$ for the Lifshitz doping seems to diverge as $\ln(1/T)$. If this behavior is followed in an extended temperature region, it would be consistent with a marginal Fermi liquid picture. The divergence of $\chi_S(\mathbf{Q} = 0, T)$ in Fig. 6 (c), as well as the enhanced antiferromagnetic fluctuations observed in Fig. 5, convey the picture that as t' goes from positive to negative values, the dominant fluctuations in the pseudogap and superconducting regions change in a very subtle manner. At $t' = 0$, charge fluctuations are strongest close to the maximum of the superconducting dome, as evident from the diverging charge susceptibility, $\chi_C(\mathbf{Q} = 0, T)$, in Fig. 6 (d). However, at $t' < 0$, the charge susceptibility at all fillings including $n_c(t'/t)$ is suppressed, and at the same time the spin susceptibility becomes more diverging. This observation is consistent with our previous results,[6,17] where we showed that charge fluctuations indeed dominate in the vicinity of the finite temperature classical critical points for $t' > 0$. However, as t' becomes negative, charge fluctuations are suppressed in the doping region corresponding to the superconducting and pseudogap states. In these parameter regime, spin fluctuations become greatly enhanced, and from Fig. 4 we see the spin component dominates the pairing interaction. Such a change of dominant fluctuations from charge to spin, as t'/t changes sign, is highly non-trivial and needs further analysis and understanding.

IV. DISCUSSION

Quantum criticality is one of the driving forces behind many of the unconventional superconductors known today. Most prominent examples are the heavy fermions based on lanthanide or actinide inter-metallics[42,43] and possibly also the iron pnictides[44,45]. For the latter materials, the QCP has been unambiguously identified as driven by spin fluctuations, although the precise mechanism – Hertz-Millis type spin-waves[46,47] or Coleman-Si type local quantum criticality[48,49] – has not been unanimously settled yet.

The situation is even worse in the case of cuprate high-T_c superconductors. Here, all experimental evidence points towards a QCP just below the dome, but its nature is completely open. There are several competing scenarios. Varma, for example, favors a loop-current type QCP, based on the analysis of the marginal Fermi liquid in terms of symmetry arguments[50,51]. The success of the spin-fluctuation approach to explain both the superconducting dome and the anomalous features above it would point towards a spin-wave type QCP, but in the region of optimal doping there is no real evidence for something along that line. Others propose some hidden

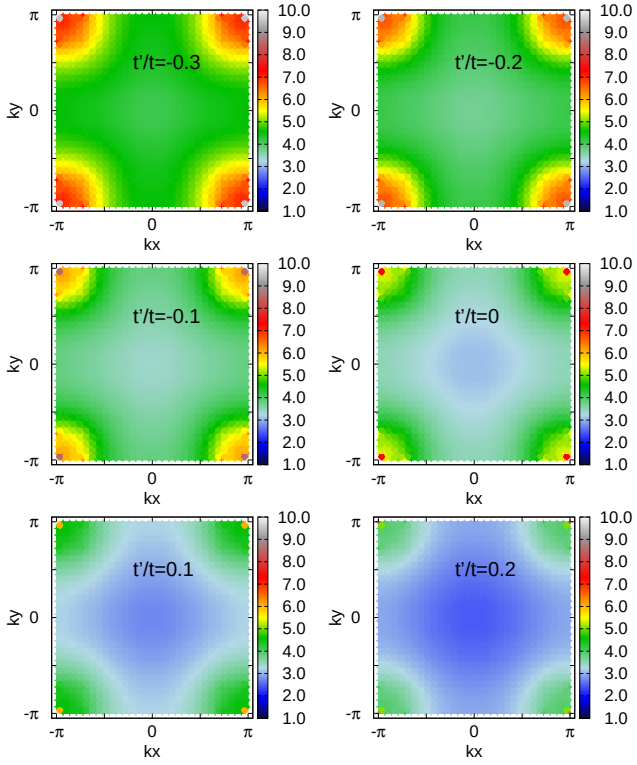

FIG. 5. (color online) Cluster spin susceptibility $\chi_S(\mathbf{Q}, T)$ for a $N_c = 16$ cluster, $n = 0.85$ and $T = 0.1t$. After interpolating the cluster spin susceptibility to the entire BZ, one clearly sees that as t'/t goes from positive to negative values, the spin susceptibility develops greater weight at $\mathbf{Q} = (\pi, \pi)$, corresponding to enhanced antiferromagnetic spin fluctuations at the negative t' side of the phase diagram.

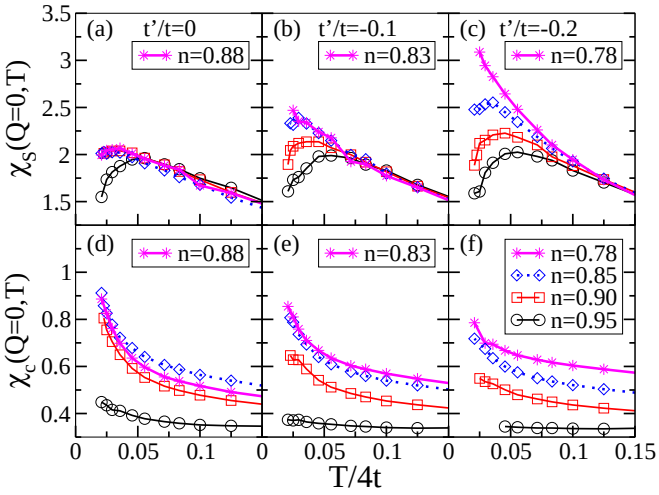

FIG. 6. (color online) (a), (b), (c) Bulk spin susceptibility ($\chi_S(\mathbf{Q} = 0, T)$) vs temperature at $t' = 0$, $t'/t = -0.1$ and $t'/t = -0.2$ and different fillings including the corresponding quantum critical Lifshitz filling, $n_c(t'/t)$ (pink stars) (d), (e), (f) Bulk charge susceptibility ($\chi_C(\mathbf{Q} = 0, T)$) vs temperature for the same values of t'/t and fillings. Results are obtained from $N_c = 16$ DCA/CTQMC simulations.

control parameter, driving the system off the QCP at the physically relevant values[52–54]. Finally, the Lifshitz transition scenario[55], possibly supported by the stripes sometimes observed[56], is another candidate.

Based on our DCA/CTQMC simulations for the two-dimensional Hubbard model, we can support a combination of the latter two scenarios. As presented in the schematic phase diagram of Fig. 7, for $t' > 0$ we indeed find a line of phase transitions between a Mott liquid and a Mott gas. The interesting point is that the QCP for this phase transition lies right at $t' = 0$, and is continued by a line of Lifshitz points for $t' < 0$, separating pseudogap and Fermi liquid regions. For not too large $t' < 0$ the system can still take advantage of the quantum fluctuations present in the vicinity of the QCP, which usually leads to superconductivity. The somewhat counter-intuitive observation however is, that the dome does not follow the Lifshitz line, but has a much weaker dependence in doping. Such a complicated behavior could however be understood by studying the pairing strength V_d (see Fig. 3). The curvature of the doping dependence of V_d changes from convex to concave function as t' changes its sign. This fixes the position of the peak of the superconducting dome to the same optimal filling of $n \approx 0.85$ for all t' studied. On the other hand, the faster decay of V_d at higher doping due to its concave curvature constraints the dome to extend to higher doping at negative t', although the Lifshitz line does so. Along the Lifshitz line, we furthermore observe that the spin fluctuations become enhanced over the charge fluctuations (see Fig. 6), which are dominant at $t' \geq 0$.

We interpret this behavior in terms of the vicinity to the Mott liquid present at $t' > 0$, which favors local moment formation and hence enhanced spin fluctuations in two-dimensions. For $t' > 0$ superconductivity is inhibited by the presence of the Mott liquid, which is adiabatically connected to the pseudogap phase for $t' \leq 0$, where the superconductivity can survive longer (left of the Lifshitz line in Fig. 7). This is due not only to the quantum critical fluctuations associated with the QCP, but a cooperation of incipient quasiparticle formation in the pseudogap phase together with surviving spin fluctuations from the latter. It is noteworthy that the Lifshitz line actually seems to be the line where superconductivity terminates or becomes dramatically suppressed; right to the Lifshitz line there are well-developed quasiparticle, but no strong enough fluctuations to support superconductivity.

V. CONCLUSION

Using large-scale dynamical cluster quantum Monte Carlo simulations, we map out the phase diagram of the two dimensional Hubbard model in the vicinity of the

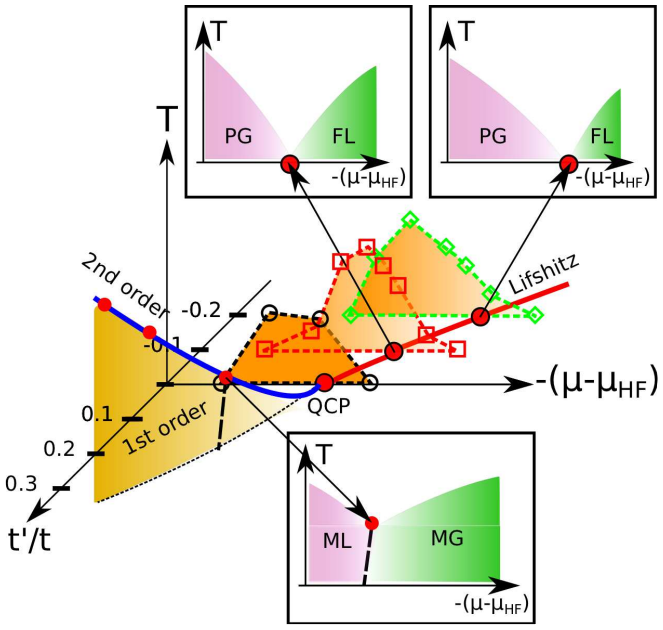

FIG. 7. (color online) Schematic phase diagram of the two-dimensional Hubbard model based on numerical data presented here and in previous publications, with temperature (T), chemical potential (μ), and next-nearest-neighbor hopping (t') as the control parameters. For clarity we neglect antiferromagnetic phases. For each t', we shift the chemical potential μ with respect to its half filling value $\mu_{\rm HF}(t'/t)$. The three insets show the cut of the phase diagram at three different $t'/t = 0.1, -0.1$ and -0.2. At positive t', the Mott liquid (ML) and Mott gas (MG) phases are separated by a first order line; at negative t', the quantum critical region separates the pseudogap (PG) and the Fermi liquid (FL) phases. This region gets wider as t' becomes more negative. The superconducting dome, determined from the divergence of the d-wave pairing susceptibility, evolves with t'/t. At $t' = 0$, the QCP roughly coincides with the center of the dome; however, as t' goes to negative values, the shape of the dome becomes less symmetric, with its peak always locates close to filling $n \approx 0.85$. However, the Lifshitz points move towards the overdoped boundary of the dome.

quantum critical filling. The control parameters of our simulation are temperature T, chemical potential, and the next-nearest-neighbor hopping t'/t. We also include extensive two-particle measurements into the simulations to measure the d-wave pairing susceptibility directly. We can determine the superconducting transition temperature T_c by extrapolating the inverse of the d-wave pairing susceptibility to zero. Then we find the superconducting dome is located around the quantum critical Lifshitz doping, and furthermore follow its evolution to the negative t' side of the phase diagram. However, the evolution of the dome is subtle, since its peak stays close to the same filling ($n \approx 0.85$), whereas the whole dome moves towards higher doping, following the trend of the Lifshitz line. The d-wave projected irreducible pairing vertex function or effective pairing strength is enhanced as t' changes from positive to negative values in the under- and optimal-doped regions. The doping dependence of the effective pairing strength, changes its curvature from convex to concave as t' goes to negative values, which fixes the position of the maximum superconducting temperature at a filling of $n \approx 0.85$ and further restricts the dome from following the Lifshitz line. The vertex decomposition via parquet equations furthermore reveals that in the negative t' side of the phase diagram, the effective pairing strength is dominated by magnetic fluctuations associated with the antiferromagnetic order at momentum transfer $\mathbf{Q} = (\pi, \pi)$. Many interesting questions still remain, particularly, the reason of the changing curvature of the effective pairing strength V_d, and the change on the character of the dominant fluctuations from charge at $t' \geq 0$ to spin at $t' < 0$, and require further detailed investigations.

ACKNOWLEDGMENTS

We would like to thank Ka-Ming Tam, Pablo Rodriguez, and Karlis Mikelsons for useful conversations. We thank Joseph Betouras, Jan Zannen, Henri Alloul, Zheng-Yu Weng and Alejandro Muramatsu for valuable discussions. This work is supported by NSF grants OISE-0952300 and DMR-0706379, and the NSF EPSCoR Cooperative Agreement No. EPS-1003897 with additional support from the Louisiana Board of Regents. TP acknowledges support by the DFG through the collaborative research center CRC 602 and the research unit FOR 1807. Supercomputer support was provided by the NSF Extreme Science and Engineering Discovery Environment (XSEDE) under grant number DMR100007, the Louisiana Optical Network Initiative, and HPC@LSU computing resources.

* kuangshingchen@gmail.com
† ziyangmeng@gmail.com

[1] M. R. Norman, arXiv:1302.3176 (2013).
[2] P. W. Anderson, P. A. Lee, M. Randeria, T. M. Rice, N. Trivedi, and F. C. Zhang, J. Phys. Condens. Matter **16**, R755 (2004).
[3] P. Phillips and M. Jarrell, Phys. Rev. Lett. **105**, 199701 (2010).
[4] H. Alloul, arXiv:1302.3473 (2013).
[5] K.-S. Chen, S. Pathak, S.-X. Yang, S.-Q. Su, D. Galanakis, K. Mikelsons, M. Jarrell, and J. Moreno, Phys. Rev. B **84**, 245107 (2011).

[6] K.-S. Chen, Z. Y. Meng, T. Pruschke, J. Moreno, and M. Jarrell, Phys. Rev. B **86**, 165136 (2012).
[7] C. M. Varma, P. B. Littlewood, S. Schmitt-Rink, E. Abrahams, and A. E. Ruckenstein, Phys. Rev. Lett. **63**, 1996 (1989).
[8] C. M. Varma, Phys. Rev. Lett. **83**, 3538 (1999).
[9] M. H. Hettler, A. N. Tahvildar-Zadeh, M. Jarrell, T. Pruschke, and H. R. Krishnamurthy, Phys. Rev. B **58**, R7475 (1998).
[10] M. H. Hettler, M. Mukherjee, M. Jarrell, and H. R. Krishnamurthy, Phys. Rev. B **61**, 12739 (2000).
[11] M. Jarrell, T. Maier, C. Huscroft, and S. Moukouri, Phys. Rev. B **64**, 195130 (2001).
[12] T. Maier, M. Jarrell, T. Pruschke, and M. H. Hettler, Rev. Mod. Phys. **77**, 1027 (2005).
[13] A. Macridin, M. Jarrell, and T. Maier, Phys. Rev. B **74**, 085104 (2006).
[14] N. S. Vidhyadhiraja, A. Macridin, C. Sen, M. Jarrell, and M. Ma, Phys. Rev. Lett. **102**, 206407 (2009).
[15] K. Mikelsons, E. Khatami, D. Galanakis, A. Macridin, J. Moreno, and M. Jarrell, Phys. Rev. B **80**, 140505 (2009).
[16] A. Liebsch and N.-H. Tong, Phys. Rev. B **80**, 165126 (2009).
[17] E. Khatami, K. Mikelsons, D. Galanakis, A. Macridin, J. Moreno, R. T. Scalettar, and M. Jarrell, Phys. Rev. B **81**, 201101 (2010).
[18] N. Lin, E. Gull, and A. J. Millis, Phys. Rev. B **82**, 045104 (2010).
[19] E. Gull, M. Ferrero, O. Parcollet, A. Georges, and A. J. Millis, Phys. Rev. B **82**, 155101 (2010).
[20] S. Sakai, Y. Motome, and M. Imada, Phys. Rev. B **82**, 134505 (2010).
[21] S.-X. Yang, H. Fotso, S.-Q. Su, D. Galanakis, E. Khatami, J.-H. She, J. Moreno, J. Zaanen, and M. Jarrell, Phys. Rev. Lett. **106**, 047004 (2011).
[22] D. Galanakis, E. Khatami, K. Mikelsons, A. Macridin, J. Moreno, D. A. Browne, and M. Jarrell, Phil. Trans. R. Soc. A **369**, 1670 (2011).
[23] G. Sordi, P. Sémon, K. Haule, and A.-M. S. Tremblay, Phys. Rev. Lett. **108**, 216401 (2012).
[24] S. Sakai, G. Sangiovanni, M. Civelli, Y. Motome, K. Held, and M. Imada, Phys. Rev. B **85**, 035102 (2012).
[25] E. Gull, O. Parcollet, and A. J. Millis, Phys. Rev. Lett. **110**, 216405 (2013).
[26] I. M. Lifshitz, Sov. Phys. JETP **11**, 1130 (1960).
[27] Y. Yamaji, M. Takahiro, and M. Imada, Phys. Soc. Jpn. **75**, 094719 (2006).
[28] M. Imada, T. Misawa, and Y. Yamaji, J. Phys.: Condens. Matter **22**, 164206 (2010).
[29] M. Imada, Y. Yamaji, S. Sakai, and Y. Motome, Ann. Phys. **523**, 629 (2011).
[30] J. E. Hirsch and D. J. Scalapino, Phys. Rev. Lett. **56**, 2732 (1986).
[31] R. S. Markiewicz, J. Phys. Chem. Solids **58**, 1179 (1997).
[32] A. N. Rubtsov, V. V. Savkin, and A. I. Lichtenstein, Phys. Rev. B **72**, 035122 (2005).
[33] T. A. Maier, M. S. Jarrell, and D. J. Scalapino, Phys. Rev. Lett. **96**, 047005 (2006).
[34] M. Jarrell and J. Gubernatis, Physics Reports **269**, 133 (1996), ISSN 0370-1573.
[35] X. Wang, E. Gull, L. de' Medici, M. Capone, and A. J. Millis, Phys. Rev. B **80**, 045101 (2009).
[36] N. Bulut, D. Scalapino, and S. White, Phys. Rev. B **47**, 6157(R) (1993).
[37] S. X. Yang, H. Fotso, J. Liu, T. A. Maier, K. Tomko, E. F. D'Azevedo, R. T. Scalettar, T. Pruschke, and M. Jarrell, Phys. Rev. E **80**, 046706 (2009).
[38] K. S. Chen, Z. Y. Meng, U. Yu, S. Yang, M. Jarrell, and J. Moreno, Phys. Rev. B **88**, 041103 (2013).
[39] T. A. Maier, M. Jarrell, and D. J. Scalapino, Phys. Rev. B **74**, 094513 (2006).
[40] C. Honerkamp and M. Salmhofer, Phys. Rev. Lett. **87**, 187004 (2001).
[41] H. Alloul, T. Ohno, and P. Mendels, Phys. Rev. Lett. **63**, 1700 (1989).
[42] G. R. Stewart, Rev. Mod. Phys. **56**, 755 (1984).
[43] H. V. Loehneysen, F. Huster, S. Mock, A. Neubert, T. Pietrus, M. Sieck, O. Stockert, and M. Waffenschmidt, Physica B-Condensed Matter **230**, 550 (1997).
[44] P. Walmsley, C. Putzke, L. Malone, I. Guillamón, D. Vignolles, C. Proust, S. Badoux, A. I. Coldea, M. D. Watson, S. Kasahara, et al., Phys. Rev. Lett. **110**, 257002 (2013).
[45] T. Shibauchi, A. Carrington, and Y. Matsuda, arXiv:1304.6387 (2013).
[46] J. A. Hertz, Phys. Rev. B **14**, 1165 (1976).
[47] A. J. Millis, Phys. Rev. B **48**, 7183 (1993).
[48] E. Abrahams and Q. Si, J. Phys.: Condens. Matter **23**, 223201 (2011).
[49] P. Gegenwart, Q. Si, and F. Steglich, Nature Physics **4**, 186 (2008).
[50] Y. He and C. M. Varma, Phys. Rev. B **85**, 155102 (2012).
[51] C. M. Varma, arXiv:1307.1494 (2013).
[52] S. Sachdev, Lecture Notes in Physics **843**, 1 (2012).
[53] S. Sachdev, M. A. Metlitski, and M. Punk, Journal of Physics: Condensed Matter **24**, 294205 (2012).
[54] M. Vojta, Adv. Phys. **58**, 699 (2009).
[55] A. Hackl and M. Vojta, New J. Phys. **12**, 105011 (2010).
[56] M. Vojta, Physica C **481**, 178 (2012).